This article has been accepted for publication in a future issue of this journal, but has not been fully edited. Content may change prior to final publication. Citation information: DOI 10.1109/TAP.2022.3168688, IEEE Transactions on Antennas and Propagation

A Fully-Printed 3D Antenna with 92% Quasi-Isotropic and 85% CP Coverage

Zhen Su, *Member, IEEE*, Kirill Klionovski, Hanguang Liao, Weiwei Li, and Atif Shamim, *Senior Member, IEEE*

***Abstract*—Internet of things (IoT) applications require orientation insensitive wireless devices to maintain stable and reliable communication. For those reasons, antennas providing a wide quasi-isotropic and circular polarization (CP) coverage are very attractive. However, achieving a wide quasi-isotropic and CP coverage simultaneously is challenging. In this work, we show that properly designed sloped dipoles on a 3D structure can maximize the CP coverage (theoretically up to 100%) even with equal-phased feed to the dipole elements. We derive the conditions and present the design graphs for the optimum slope angle for the dipole elements on a 3D hexagonal-shaped package to achieve a wide quasi-isotropic and CP coverage simultaneously. Based on the proposed theory, a practical antenna has been designed and fabricated using additive manufacturing. The measured results demonstrate a 7dB-isotropy of 92% and a CP coverage of 85%, which matches well with the predicted results from the theoretical analysis and full-wave simulations.**

***Index Terms*— circularly polarized antenna; quasi-isotropic radiation pattern; Orientation insensitive antenna.**

I. INTRODUCTION

LAST few decades have seen Internet of things (IoT) emerging as a new paradigm where billions of wireless sensor nodes are expected to communicate with each other [1-3]. In such IoT applications, the antenna is desired to be low-cost, light-weight, space-efficient, and orientation-insensitive. Inspired from Antenna on package (AoP) concept in the semiconductor industry, designing antennas on IoT devices' packages can save cost and space for IoT applications, as the package not only provides the necessary cover and protection for the electronics but also functions as the antenna substrate [4-6]. Additional cost-savings can be done through additive manufacturing (AM) techniques where material wastage is minimized through digital operations as compared to the traditional subtractive manufacturing techniques[7, 8]. Orientation-insensitive radiation performance of antennas is important for IoT applications since the wireless sensor nodes may be placed or dispersed in random orientations. To avoid communication outage, the antenna must, ideally, radiate equally in all directions (perfect isotropic radiation pattern). However, the perfect isotropic radiation pattern is very difficult to achieve in practice, so efforts are being made to achieve a radiation pattern as close to the isotropic pattern as possible (by maximizing the isotropy coverage), and this is typically known as quasi-isotropic radiation pattern. In addition, for multi-path or harsh environments, CP waves are considered to provide better stability as compared to linear polarization waves [9], and this can help IoT devices' communication in such complex environments. Thus, maximizing CP coverage in the 3D radiation sphere is also an important aspect for IoT antennas. The issue is that achieving both, quasi-isotropic radiation pattern and wide CP coverage is quite challenging [10].

In the published literature, some antenna designs with quasi-isotropic radiation patterns have been reported [11-22]. The quasi-isotropy in radiation patterns is achieved by various mechanisms, such as folded dipoles [12-16], split-ring resonators [17-20], and a combination of electric dipoles with slot antenna [21]. However, these works are directed towards achieving the quasi-isotropic radiation pattern, and no attention is paid to achieving CP coverage. On the other hand, there are papers focusing only on enhancing the CP coverage by various methods, like meandered dipoles [23, 24], cavity-backed antennas [25], or conical log spiral antennas [26]. Although some of them have very wide CP coverage, the radiation patterns are not isotropic. Very few works have been reported that have attempted to achieve quasi-isotropic radiation patterns and wide CP coverage at the same time [27-32]. However, [28-30] have a directional radiation pattern for each polarization sense, i.e., RHCP radiation in one semi-sphere and LHCP in the other semi-sphere. Thus, they are not orientation-insensitive and not very suitable for IoT applications. We have recently investigated the conditions for achieving near-isotropy and wide CP coverage radiation simultaneously [31]. We have shown that by optimizing the phase conditions for three-orthogonal dipoles, a maximum CP coverage of 21% and a 7dB-isotropy coverage of 98% can be obtained theoretically.

Though we achieved a decent 7dB-isotropy coverage in [31], the obtained CP coverage was limited. In this paper, we introduce ring current model and optimize the CP coverage through the slope angles instead of the applied phases. We derive the conditions for the optimum slope angle for the uniform

H. Liao, W. Li and A. Shamim are with the Computer, Electrical and Mathematical Sciences and Engineering Division, King Abdullah University of Science and Technology (KAUST), Thuwal, 23955-6900, Saudi Arabia.(email: Hanguang.liao@kaust.edu.sa)

Z. Su and K. Klionovski were with the Computer, Electrical and Mathematical Sciences and Engineering Division, King Abdullah University of Science and Technology (KAUST), Thuwal, 23955-6900, Saudi Arabia. Now Z. Su is with Antenna and RF team in Wearable Sensor Network Group, Tyndall National Institute, Cork, T12R5CP, Ireland, (email: zhen.su@tyndall.ie), and K. Klionovski is with the Department of Information Engineering and Mathematics, University of Siena, 53100 Siena, Italy (email: kirill.klionovski@unisi.it).

This article has been accepted for publication in a future issue of this journal, but has not been fully edited. Content may change prior to final publication. Citation information: DOI 10.1109/TAP.2022.3168688, IEEE Transactions on Antennas and Propagation

ring current model to achieve wide isotropy and CP coverage simultaneously and conclude the analysis into a simple design equation. It is shown that while maintaining > 90% quasi-isotropy, the CP coverage can be maximized to 100% (theoretically), even with equal-phase feeding. Based on the developed theory, an antenna prototype has been designed and realized through AM, which demonstrates a CP coverage of 85% and a 7-dB isotropy coverage of 92.6%, showing a significant improvement in our previously reported results [31].

II. Theoretical Model

This section focuses on the theoretical considerations for maximizing the CP coverage. It will be shown that 100% CP coverage can be achieved by combining electrical and magnetic dipole moments with equal-phase feeding. First, the definition of isotropy and CP coverage is introduced, and then, the analytic expressions for the antenna model are derived. Two design graphs and a simple design equation is also proposed based on the theoretical model, which is useful for designers who are interested in wide isotropy and CP coverage antennas.

A. Definition of isotropy and CP coverage

The integral isotropy factor is calculated by finding the ratio of the surface where the gain deviation exceeds the threshold gain level, 7 dB, over the whole radiation sphere [31, 33]. The 7 dB threshold level for evaluating quasi-isotropy has previously been utilized by many published works [34-37]. The sum of the beams solid angles whose gain between the peak gain (PG) and PG -7dB is a measure of the radiation pattern isotropy, where these beams are considered to have effective radiation. This can be expressed mathematically by an integral parameter I^{th-iso} as equation (1.a) below.

$$I^{th-iso} = 100\% \times \iint_{S_1} \frac{\sin\theta d\theta d\varphi}{4\pi}, \tag{1.a}$$

The surface S_1 is determined by

S_1 such that $PG - 7dB \le Gain(\theta, \varphi) \le PG$.

Similarly, the sum of the radiation pattern beam solid angles that satisfies axial ratio (AR) in the range of $1 \le AR(\theta, \varphi) \le \sqrt{2}$ relative to the whole radiation sphere is a measure of the radiation pattern CP, which is expressed mathematically by the equation (1.b) below [31].

$$I^{CP} = 100\% \times \iint_{S_2} \frac{\sin\theta d\theta d\varphi}{4\pi}, \tag{1.b}$$

The surface S_2 is determined by

S_2 such that $1 \le AR(\theta, \varphi) \le \sqrt{2}$.

B. The model for obtaining 100% CP coverage

The model combines the z-oriented Hertzian electric $\mathbf{j}_z^e$ and magnetic $\mathbf{j}_z^m$ dipoles located at the origin, which are characterized by electric p_e and magnetic p_m dipole moments. Note that in this paper, all the E-field patterns are far-field results, and the $\frac{e^{-ikr}}{r}$ term is ignored in all the analytic expressions for simplicity purposes. The radiation pattern of the electric and magnetic dipole has the following meridional E_θ and azimuthal E_φ components of the electric field intensity,

$$E_\theta(\theta) = \frac{ip_e kZ_0}{4\pi}\sin\theta, \tag{2.a}$$

and

$$E_\varphi(\theta) = -\frac{ip_m k}{4\pi}\sin\theta, \tag{2.b}$$

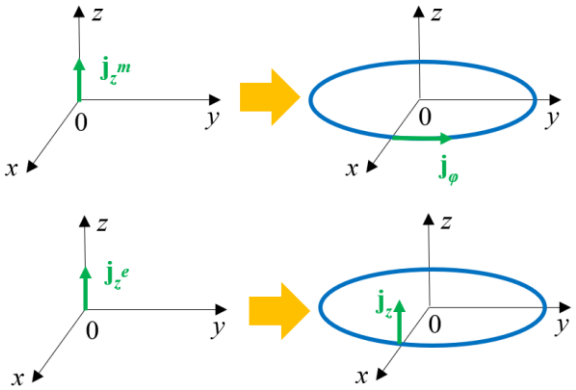

Fig. 1 The ideal dipoles' replacement.

respectively. Here, Z_0=120π Ω, which is the free space wave impedance; k=2π/λ; where λ is the radiation wavelength in free space; and i is the imaginary unit. From equations (2.a, 2.b), we can see that pure circular polarization at all directions (100% CP coverage) can be obtained when the electric and magnetic dipole moments are combined under the condition, p_e=±ip_m/Z_0. This means that in order to obtain perfect CP coverage, we can adjust the excitation of the electrical and magnetic dipole to match with p_e=±ip_m/Z_0. Further, for orientation-insensitive antennas, it is important to verify the isotropy performance in the 3D radiation sphere (refer to equation (1.a)). It is well known that both Hertzian electric and magnetic dipoles have the same donut-shaped radiation patterns (E-field proportional to sinθ, see equation 2). So, if p_e=±ip_m/Z_0, for 100% CP coverage, the combined radiation pattern is proportional to $2\sin^2\theta$, which still results in a donut-shaped pattern. Using equation (1.a), the 7-dB isotropy coverage for such radiation pattern ($2\sin^2\theta$) is 89.5%. From the theoretical analysis for Hertzian electrical and magnetic dipole model, we can conclude that using the combination of electrical and magnetic dipoles, a 100% CP coverage and 89.5% 7dB isotropic coverage can be obtained theoretically. However, Hertzian dipoles are ideal antennas with infinitesimal length and cannot be used for practical applications. We will show that the Hertzian dipoles can be replaced with ring currents and similar performance can still be achieved.

It is known that the magnetic dipole moment is generally realized by a small circular current. To transform the ideal model into a practical antenna design, we replace the electric dipole and magnetic dipole to a ring of axial $\mathbf{j}_z=\delta(\rho-R)\delta(z)\hat{\mathbf{z}}$ and azimuthal $\mathbf{j}_\varphi=\delta(\rho-R)\delta(z)\,\hat{\boldsymbol{\varphi}}$ electric current of radius R, respectively, as shown in Fig. 1. Here, $\delta(z)$ is the Dirac delta function; $\hat{\boldsymbol{\varphi}}$ and $\hat{\mathbf{z}}$ are the unit azimuthal and axial-vector in the cylindrical coordinates (ρ, φ, z), respectively. The radiation pattern of the axial and azimuthal ring current has the following components,

$$\mathrm{E}_\theta(\theta) = i\,\frac{kRZ_0}{2}\sin\theta J_0(kR\sin\theta) \tag{3.a}$$

and

$$\mathrm{E}_\varphi(\theta) = \frac{kRZ_0}{2}J_1(kR\sin\theta) \tag{3.b}$$

This article has been accepted for publication in a future issue of this journal, but has not been fully edited. Content may change prior to final publication. Citation information: DOI 10.1109/TAP.2022.3168688, IEEE Transactions on Antennas and Propagation

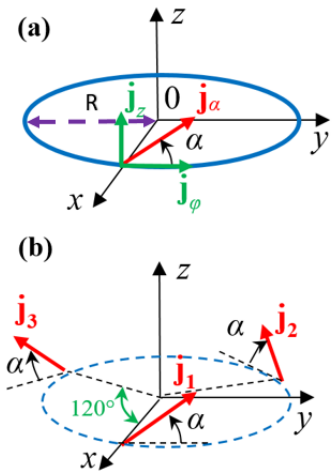

Fig. 2 (a) ring current model and (b) its 3 dipoles' approximation.

respectively. Here, $J_n(kR\sin\theta)$ is nth order Bessel function of the first kind and argument $kR\sin\theta$.

The axial and azimuthal current components are orthogonal to each other, and they can be used to analyze the current on the cylinder surface. Let us consider a ring of uniform electric current which has an angle "α" on the cylinder surface with respect to the azimuthal plane. The uniform inclined ring current $\mathbf{j}_\alpha$ can be decomposed as $\mathbf{j}_\alpha = \mathbf{j}_\varphi\cos\alpha + \mathbf{j}_z\sin\alpha$, using the axial and azimuthal currents, as shown in Fig. 2 (a). Thus, the radiation pattern of the ring current $\mathbf{j}_\alpha$ has the following two orthogonal components:

$$E_\theta(\theta) = i\,\frac{kRZ_0}{2}\sin\theta J_0(kR\sin\theta)\sin\alpha \quad (4.a)$$

, and

$$E_\varphi(\theta) = \frac{kRZ_0}{2}J_1(kR\sin\theta)\cos\alpha \quad (4.b).$$

There are two parameters, radius "R*"* and inclined angle "α", in the inclined ring current model that can be chosen to optimize the CP performance (see Fig. 2(a)). For this purpose, the maximum value of AR (termed as AR_{max}) has been calculated for various "R*"* and "α" combinations, as can be seen in Fig. 3(a). Every point (R, α) in Fig, 3(a) represents a unique ring current design. The AR_{max} at point (R, α) represents the largest AR value in the entire 3D radiation sphere for all φ and θ (AR_{max} = max{AR(φ, θ)}). If the AR_{max} is smaller than 3dB, it means that for this particular design (R, α), CP radiation can be achieved for any φ and θ in the entire 3D radiation sphere, or in other words, 100% CP coverage can be achieved. This boundary of AR_{max} =3 dB is shown in Fig. 3(a) with a solid black line, and within this boundary (dark blue region), all the designs (R, α) can theoretically have a 100% CP coverage. The opposite is true for all the designs (R, α) outside this boundary (red and green regions). For example, if we choose R=0.2λ, α can be chosen between 30° to 42° to obtain 100% CP coverage, as shown in Fig. 3(a) with a dashed purple line. Any point below or above this range of α in the light blue and green part will still have a certain CP coverage but not 100% CP coverage. Going beyond that (in the red and green region), the polarization coverage is mostly elliptical or linear. This can be clearly seen in Fig. 3(b), where AR pattern in the elevation plane for three different values of α. We can see that AR < 3 dB for all θ values if α = 36° and, thus, we get 100% CP coverage. For the other

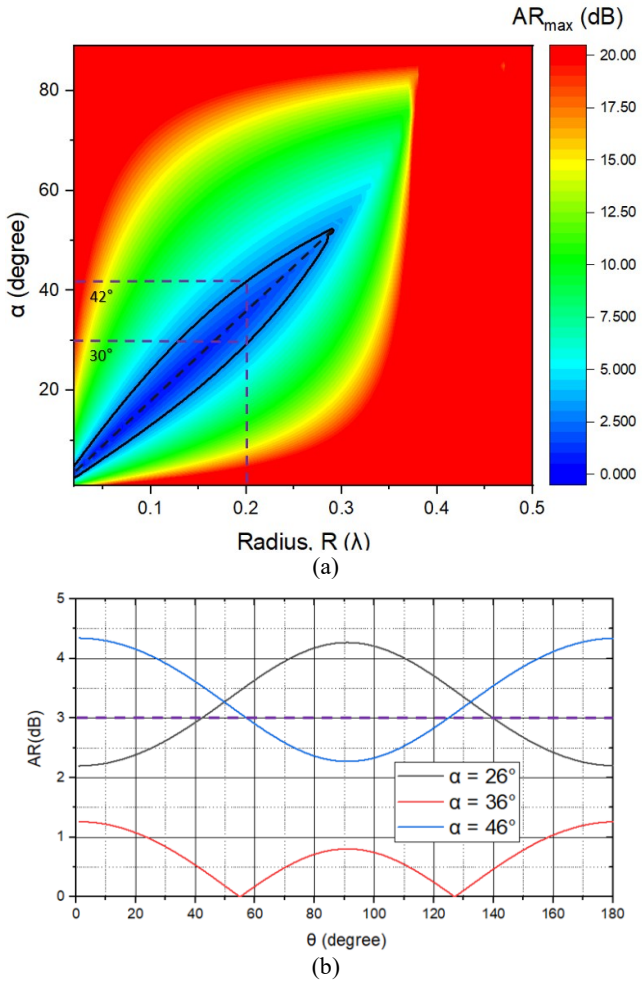

Fig. 3 CP performance study: (a) maximum AR over the radiation sphere for various radius and α (100% CP coverage region within the black solid line); (b) AR pattern with various α for radius $R = 0.2\lambda$.

two values of α, i.e., 26° or 46°, there are some values of θ where the CP condition is not met (AR > 3 dB), as the curves go above the purple dashed line in Fig.3 (b).

From Fig. 3(a), we can see that the perfect CP region (AR_{max} < 3 dB) is restricted in R < 0.3λ, which means to obtain 100% CP coverage from the inclined ring current designs, the radius of the ring cannot exceed 0.3λ. This is because when R becomes larger, the ring current cannot be accurately represented by a magnetic dipole moment. This aspect can also be seen in a circular loop antenna with uniform current distribution, where the donut-shaped radiation pattern gets distorted when the radius increases to $\frac{R}{\pi}$, since the $J_1(kR\sin\theta)$ term in equation (3.b) approaches its first pole [38]. It is also worth mentioning here that the black dashed line through the center of the 100% CP coverage region (AR_{max} < 3 dB region) in Fig. 3(a) is almost linearly proportional to R. A simple linear fitting of this dashed line results in the formula given in (5), which can be used for such designs:

$$\alpha = 177.1 * R + 1.4, for\ R < 0.3\lambda \quad (5)$$

where α is in degree, and R is in λ. The use of this design equation will be shown in Section III.

This article has been accepted for publication in a future issue of this journal, but has not been fully edited. Content may change prior to final publication. Citation information: DOI 10.1109/TAP.2022.3168688, IEEE Transactions on Antennas and Propagation

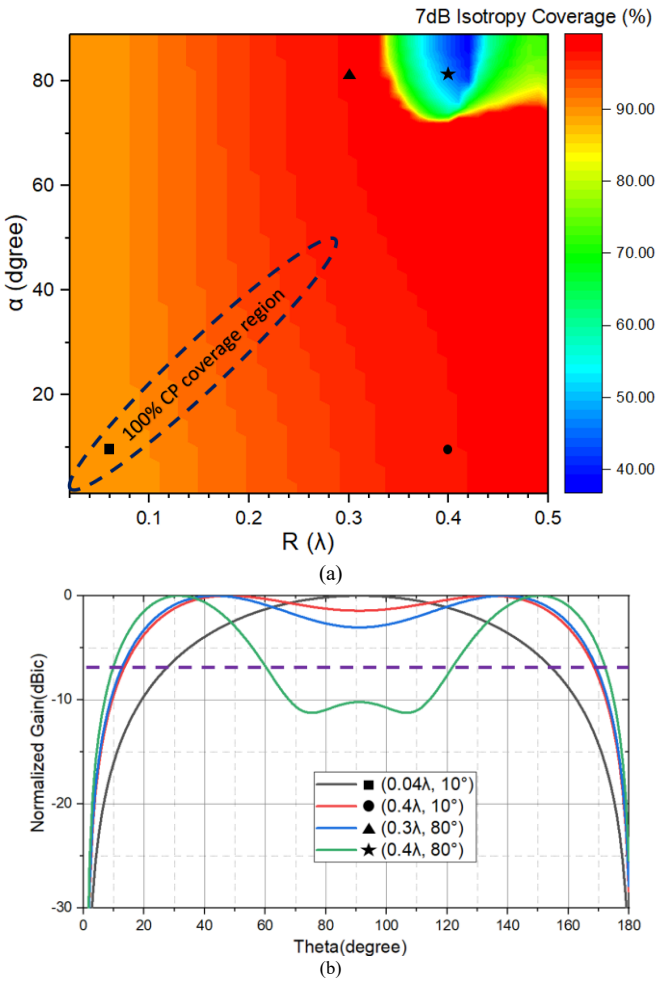

Fig. 4 Isotropy performance study: (a) 7dB isotropy coverage; (b) normalized radiation pattern for few examples (R, α).

The quasi-isotropy performance of the ring current model (shown in Fig. 2 (a)) has also been investigated. Similar to the CP performance graph, the calculated 7 dB isotropy coverage graph is shown in Fig. 4 (a). We can see that for all design combinations (R, α), where R < 0.32λ or α < 70°, a decent 7dB isotropy coverage can be obtained (> 89.5%), shown in orange and red colors in Fig. 4 (a). The 7dB isotropy coverage increases from 89.5% to 98.8%, as R increases from 0.02λ to 0.5λ, provided the α < 70°. This can also be explained with the help of radiation patterns shown in Fig. 4 (b). For designs where R < 0.1λ, the current ring can be considered as a small loop, and thus the radiation pattern must be identical to that of a magnetic dipole. For one of such designs (R=0.04λ, α =10°), the resultant 7 dB isotropy coverage is 89.5%, as shown in Fig. 4 (b). When R increases to 0.4λ, the radiation pattern becomes different from the typically obtained donut-shape, as can be seen for design (0.4λ, 10°) in Fig. 4 (b). Here, a wider 7dB power beamwidth has been achieved as compared to the design (0.04λ, 10°). There is a region in Fig. 4(a), shown in green and blue (region R > 0.32λ and α > 70°), where the designs (R, α) have a lower 7dB isotropy coverage (< 70%). This can also be verified from the radiation pattern for the design (0.4λ, 80°) in Fig. 4 (b). The radiation pattern for design (0.4λ, 80°) is not within 7dB gain variation range between 60° < θ < 120°. This decrease in gain is caused by its E_θ component (the major polarization component at α = 80°), which has nulls when θ is close to 70° and 110°, matched with the zeros of $J_0(kRsin\theta)$ in equation (4.a). This can be avoided easily in two ways, 1) use either a smaller α, or 2) a smaller radius R, as can be seen with the design combinations (0.4λ, 10°), (0.3λ, 80°) in Fig. 4 (a, b). It is worth mentioning here that the 100% CP coverage region is completely inside the high 7dB isotropy coverage region, shown in Fig. 4(a). This means that a designer can choose designs with both 100% CP coverage as well as a high isotropy coverage > 89.5%. The design equation (5) can help achieve a 100% CP coverage antenna with almost > 90% 7 dB isotropy coverage. With such CP and isotropy performance, orientation-insensitive antenna designs can be done with ease through the proposed theory and design equation.

However, realizing the uniform ring current with a specific inclined angle is challenging for practical antenna designs. We made some approximations for the ring current model in Fig. 2(a), and simplified it into a three-dipole model in Fig. 2(b). Numerical analysis (shown in the next section) confirms that 100% CP coverage can also be obtained through an approximation of the ring current $\mathbf{j}_\alpha$ by 3 dipoles $\mathbf{j}_{1,2,3}$, which are located on a circle of radius a with the equal angular spacing of 120° along the φ-axis (Fig. 2(b)).

III. Antenna Design

In this section, a practical IoT antenna is designed based on the theoretical model presented in the last section. The center frequency of the antenna is arbitrarily chosen to be 1.5 GHz, and the sense is set to be left-handed CP (LHCP). Fig. 4 (a) shows that the design (0.29λ, 52°) offers the best combination for quasi-isotropic coverage (97.2%) and CP coverage (100%). However, the radius of the antenna (~0.3 λ) and the resultant size is relatively large for this particular design. So, for a practical demonstration in this work, we choose R = 0.16λ, which still provides a 100% CP coverage and a good isotropy coverage (92.4%) but with a much smaller antenna size (80.4% volume reduction as compared to the design with R = 0.29λ). Initially, the three ideal short dipoles (Hertzian) are considered in the simulation model in Ansys HFSS, and then the practical antenna design based on the theoretical model is presented.

A. Three-Hertzian-Dipole Antenna: HFSS Model

To verify the three-sloped-dipoles approximation model, three Hertzian dipoles are placed at (R, 0, 0), (-R/2, R/2*$\sqrt{3}$, 0), and (-R/2,-R/2*$\sqrt{3}$, 0) on a circle with a radius of R = 32 mm (0.16λ), as shown in Fig. 5 (a). Using equation (5), we can calculate the best α to be equal to 30°. The three dipoles have the same slope angle from the azimuth plane, as well as the same excitations (in terms of both magnitude and phase). Note that the direction of the current's horizontal component here is opposite to that in Fig. 2(a), since we are targeting LHCP in this design.

The simulation results of the three-Hertzian-dipole model in HFSS are shown in Fig. 5 (b, c). From the AR pattern in Fig. 5(b), we can see that for all directions, we have AR < 3 dB, except nulls at θ=0° and 180°. The simulated gain pattern for

This article has been accepted for publication in a future issue of this journal, but has not been fully edited. Content may change prior to final publication. Citation information: DOI 10.1109/TAP.2022.3168688, IEEE Transactions on Antennas and Propagation

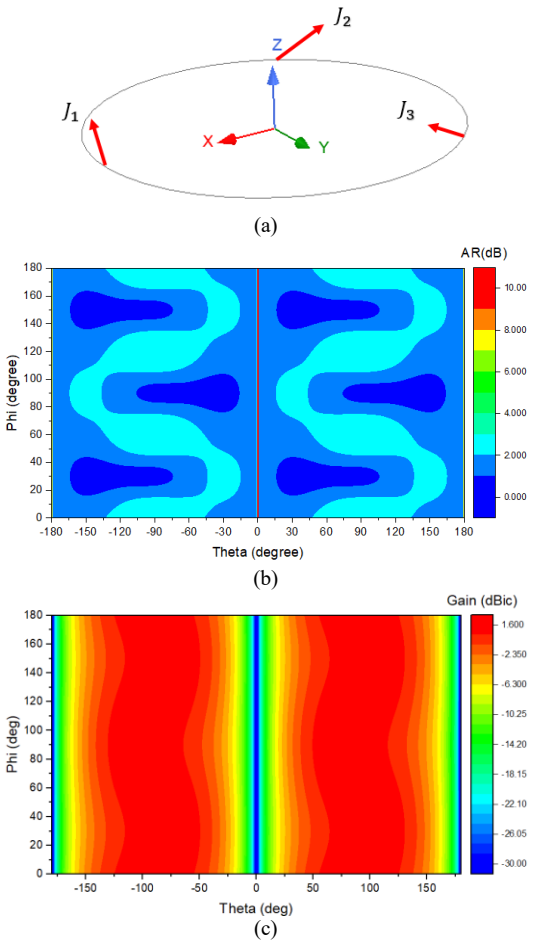

Fig. 5 Three-Hertzian-dipole model: (a) simulation model; (b) AR pattern; (c) gain pattern.

the three-Hertzian-dipole model is shown in Fig. 5(c). We can see LHCP everywhere is the radiation sphere, except for the two nulls, near θ=0° and 180°. The simulated far-field data is then used in equation (1.a, 1.b) to calculate the CP coverage and near isotropy of the Hertzian dipole model. A CP coverage of 99%, and the 7dB quasi-isotropy coverage of 92.6% is obtained, which matches well with the theoretical analysis of the ring current model presented in the in last section (see Fig. 4 (a)). It also proved that the ring current model could be replaced by its three-dipole approximation model, with similar isotropy and CP performances. Moreover, the feasibility of the proposed design equation (5) is also verified successfully. It is worth mentioning that the sense of CP polarization (LHCP or RHCP) can be switched simply by change α value to its supplementary angle value.

B. Practical IoT Antenna design

In this section, the three-Hertzian-dipole model is transformed into a practical antenna which is suitable for IoT applications. For practical antenna designs, half-wavelength dipoles are more suitable due to the good radiation efficiency and ease in impedance matching. The antenna is realized on a hexagonal prism package, which provides a suitable structure to accommodate the three half-wavelength dipoles separated by 120° between each other, as shown in Fig. 6(a). The package

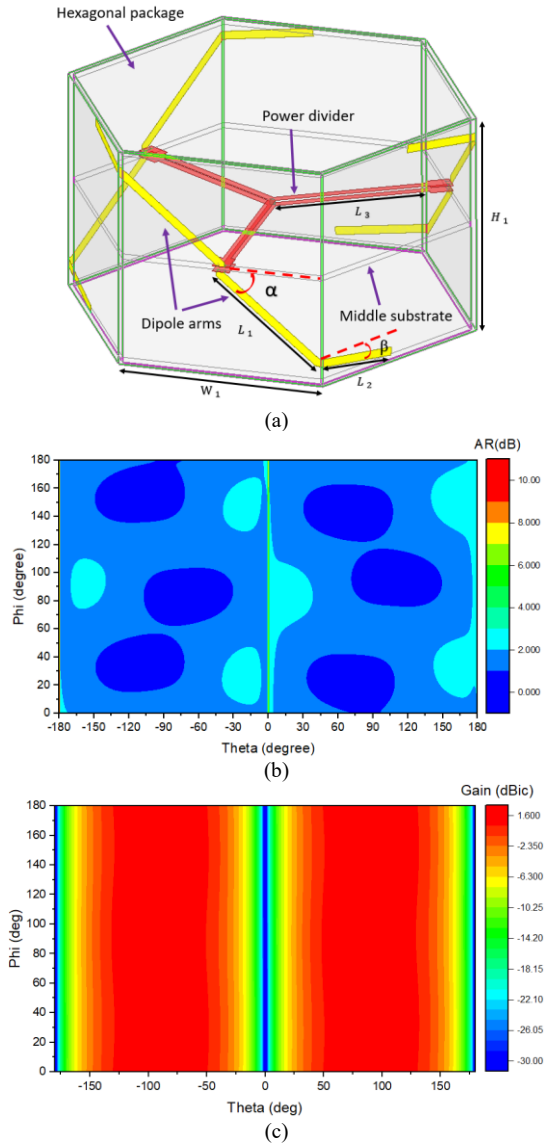

Fig. 6 Practical IoT antenna design: (a) HFSS simulation model; (b) AR pattern; (c) gain pattern. Dimensions: L_1=21.7 mm, L_2=14.8 mm, L_3=26.5 mm, α=34°, β=12°, H_1=40 mm, W_1=37.5 mm.

and the substrate in the middle are using 3D printable filaments, namely PREFERM® ABS300 (dielectric constant of 3.0 and loss tangent of 0.004). The printed package walls and the middle substrate have a thickness of 1 mm, as a compromise between robustness and dielectric loss. The metallic traces are planned to be screen printed on the substrate using conductor paste DuPont PE819, with a conductivity around 5×10^6 S/m. The width of all the dipole arms is 1.5 mm, and the optimized dimension for other parameters are shown in the caption of Fig. 6. It is worth mentioning here that α=34° is slightly different from the calculated value of 30°. This is because the hexagonal structure in the practical design is different from the ideal circle used in the analytic calculations, where the edge-to-center distance is always constant. In the hexagonal structure, the closest edge-to-center distance is 32mm, while the corner-to-center distance is 37.5 mm. This means that our optimum sloped angle should be chosen between 30° and 35° (for R = 32 and 37.5mm), and α=34° is the optimized value found through

This article has been accepted for publication in a future issue of this journal, but has not been fully edited. Content may change prior to final publication. Citation information: DOI 10.1109/TAP.2022.3168688, IEEE Transactions on Antennas and Propagation

simulations. For the second wrap of the dipole arm on the hexagonal structure, ideally the slope angle should also be 30°. However, this will result in a larger structure. Thus, simulations have been done to investigate the effect of this angle (termed as β in Fig. 6(a)) on the radiation performance. It has been found that β does not impact the far-field pattern significantly because the current in that arm is minimum, thus β=12° has been selected to ensure a compact design. The three dipole antennas are connected to a 3-way power divider based on quarter-wavelength parallel strips (width of 1.4 mm), shown in red in Fig. 6(a).

The simulated AR and gain patterns are shown in Fig. 6(b, c). If we compare these results with that of the three-Hertzian-dipole model in Fig. 5(b, c), the two results appear to be identical. We can see LHCP in the entire radiation sphere except the two nulls. The calculated CP coverage is 99%, and the 7dB isotropy coverage is 92.4% across the entire radiation sphere. This validates the proposed theory for simultaneously achieving a nearly full CP coverage as well as a high isotropy coverage.

IV. Fabrication and Experimental Results

A. Fully Printed Manufacturing

The antenna prototype is fabricated through a fully printed process, i.e., 3D printing with PREFERM® ABS300 filament, and screen-printing using DuPont PE819 conductor paste, as has been illustrated in Fig. 7 (a). The six sidewalls of the hexagonal package, which also acts as the substrate for the antenna, have been 3D printed as a single piece by Raise 3D Pro2 printer. The middle, top, and bottom walls of the package have been separately printed. The middle piece/substrate carries the feed lines. The mask for each metallic pattern is cut by laser, which can be reused for multiple prototypes. The metallic patterns are screen printed on these 3D printed substrates, and cured in an oven at 70 °C for two hours. In the final stage, the six side walls are wrapped in the form of a hexagonal and the top, bottom and middle parts are attached with the hexagonal structure through a super glue. Due to additive manufacturing, not only material wastage is avoided, but the IoT antenna is also quite lightweight (19.0 grams only). The final fully printed antenna prototype is shown in Fig. 7 (b).

B. Characterization

To measure the differential antenna using single-ended equipment, a balun is needed between the antenna and the coaxial cable. Thus, a Bazooka balun (length of 42 mm and radius of 10 mm) is built and is placed half-wavelength (96mm) away from the antenna, as shown in Fig. 8(a). However, the presence of the balun causes spurious radiations, which is detrimental for radiation performance. Thus, the balun, is covered with an absorber layer (dielectric constant of 15, electric loss tangent of 0.2, magnetic loss tangent of 1), as can be seen in Fig. 8(a).

To check if the proposed measurement setup has any effect on antenna performance, the complete test setup in Fig. 8(a) is simulated in HFSS. It is observed that the CP and quasi-isotropic performance is somewhat changed due to the presence

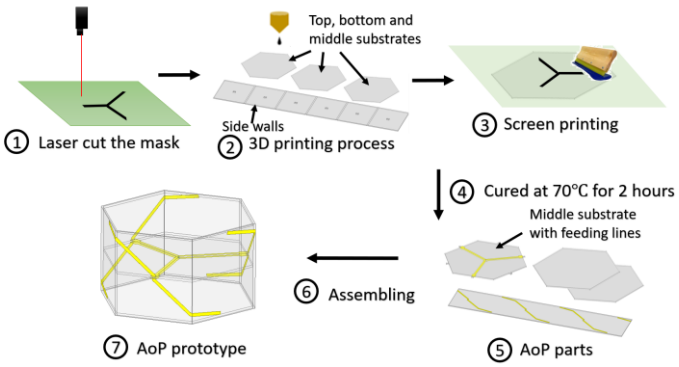

(a)

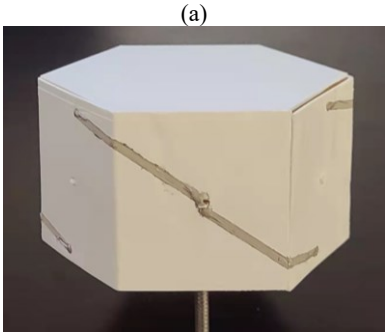

(b)

Fig. 7 (a) Fabrication process, and (b) fabricated antenna prototype.

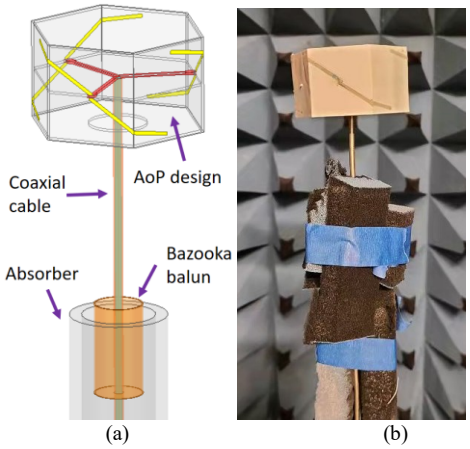

(a) (b)

Fig. 8 Antenna with cable and balun: (a) HFSS simulation model; (b) test in anechoic chamber.

of coaxial cable, balun, and absorber. The CP coverage and the 7dB-isotropy coverage with the balun is 89% and 92.4%, respectively in simulations, which is lower as compared to the antenna simulation model. The decrease in the CP coverage is because of the spurious radiation from the uncovered coaxial cable (shown in Fig. 8 (a)). Part of the coaxial cable is left uncovered on purpose because covering it with the absorber has negative effect on the overall radiation performance of the antenna, particularly the radiation efficiency.

The S parameter of the antenna (with the complete test setup) is measured by Keysight N9912A network analyzer, and shown in Fig. 9. The measured impedance bandwidth of the antenna is 130 MHz (8.6%), centered at 1485 MHz, and generally has a decent match with the simulated results, and only a small frequency shift of 1.5% has been observed as compared to the simulated results. The radiation performance is measured in Satimo StarLab anechoic chamber, and the setup is shown in

This article has been accepted for publication in a future issue of this journal, but has not been fully edited. Content may change prior to final publication. Citation information: DOI 10.1109/TAP.2022.3168688, IEEE Transactions on Antennas and Propagation

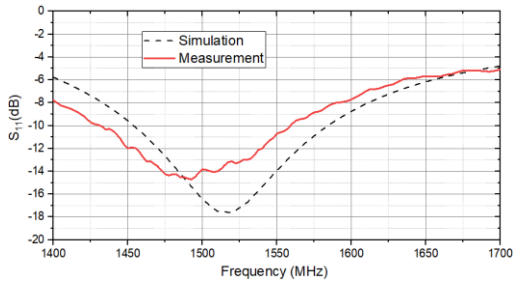

Fig. 9. Measured S parameters of the total antenna system.

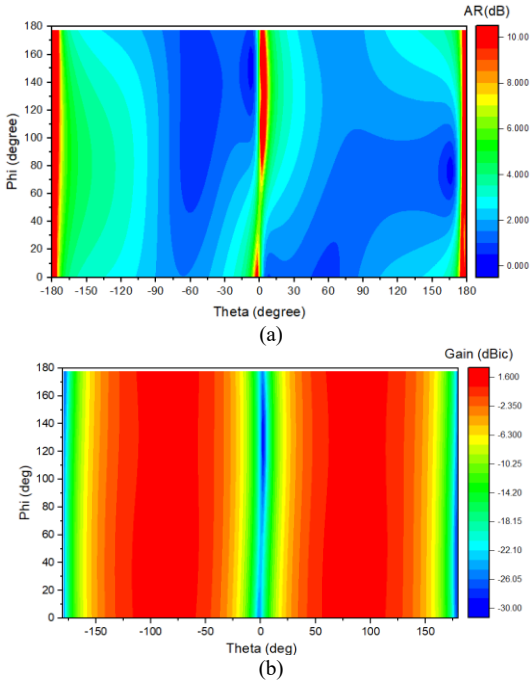

Fig. 10 Measured results: (a) AR pattern; (b) gain pattern.

Table I. Summarized isotropy and CP performace for antenna evolution.

	7dB isotropy Coverage	CP coverage
Thoerectical model	>89.5%	100%
Hertzian dipole model	92.6%	99%
IoT antenna design	92.4%	99 %
Antenna with cable and balun (simulation)	92.4%	89%
Antenna with cable and balun (measurement)	92.6%	85%

Fig. 8(b). The measured AR and gain patterns are shown in Fig. 10. The measured pattern data is then calculated, showing a CP coverage of 85%, which is 4% lower as compared to the simulated results. The measured 7dB isotropy coverage is 92.6%, with a peak gain of 1.66 dBic at 1.48 GHz. The measured radiation efficiency is 88% at 1.48 GHz, even with the presence of absorbers, which is considered to be quite high for fully printed RF electronics [39]. The slight deviation between the simulated and measured results can be caused by fabrication tolerances, particularly in the case of 3D printed parts.

The CP and isotropy performance has been summarized in Table I. From this table, we can see that the isotropy performance has stayed consistent from the theoretical stage to the practical design stage. However, the CP coverage has degraded somewhat because of the presence of the cable and the balun. It is worth mentioning here that, for IoT applications, where the antenna is fed by the integrated electronics and not through the cable and balun combination, the negative effects due to the cable and balun can be avoided.

V. Conclusions

In this paper, a fully printed antenna with simultaneously optimized quasi-isotropic and CP coverage is proposed. A ring current model is proposed to obtain 100% CP and wide isotropy coverage. A simple design equation has been derived to design antennas with 100% CP and wide isotropy coverage. Full-wave simulation results for a simplified three-dipole approximation model and a practical IoT antenna design verify the proposed theory and the design equation. The antenna is manufactured using a combination of 3D as well as screen printing techniques. The measured results from the prototype align well with the simulation results, except few minor variations. The presence of the cable and balun does affect the antenna radiation performance negatively. However, they are only required for testing and will not be part of the practical antenna system where the feed to the antenna is through the integrated driving circuits. The proposed theoretical model, design equation and the design of the fully printed antenna are important milestones for futuristic efficient antenna systems in the IoT realm.

VI. References

[1] S. N. Swamy and S. R. Kota, "An Empirical Study on System Level Aspects of Internet of Things (IoT)," IEEE Access, vol. 8, pp. 188082-188134, 2020.

[2] W. Zhou, Y. Jia, A. Peng, Y. Zhang, and P. Liu, "The effect of iot new features on security and privacy: New threats, existing solutions, and challenges yet to be solved," IEEE Internet of Things Journal, vol. 6, no. 2, pp. 1606-1616, 2018.

[3] I. Lee and K. Lee, "The Internet of Things (IoT): Applications, investments, and challenges for enterprises," Business Horizons, vol. 58, no. 4, pp. 431-440, 2015.

[4] D. Liu and Y. Zhang, Antenna-in-package Technology and Applications. John Wiley & Sons, 2020.

[5] A. Shamim and H. Zhang, "Antenna-in-package Designs in Multilayered Low-temperature Co-fired Ceramic Platforms," in Antenna - in - Package Technology and Applications, 2020, pp. 147-178.

[6] M. F. Farooqui, M. A. Karimi, K. N. Salama, and A. Shamim, "3D-Printed Disposable Wireless Sensors with Integrated Microelectronics for Large Area Environmental Monitoring," Advanced Materials Technologies, https://doi.org/10.1002/admt.201700051 vol. 2, no. 8, p. 1700051, 2017/08/01 2017, doi: https://doi.org/10.1002/admt.201700051.

[7] K. V. Wong and A. Hernandez, "A review of additive manufacturing," International scholarly research notices, vol. 2012, 2012.

[8] G. McKerricher, M. Vaseem, and A. Shamim, "Fully inkjet-printed microwave passive electronics," Microsystems &

Nanoengineering, vol. 3, no. 1, p. 16075, 2017/01/30 2017, doi: 10.1038/micronano.2016.75.

[9] C. C. Counselman, "Multipath-rejecting GPS antennas," Proceedings of the IEEE, vol. 87, no. 1, pp. 86-91, 1999, doi: 10.1109/5.736343.

[10] G. H. Brown and O. M. Woodward, "Circularly-polarized omnidirectional antenna," RCA Review, vol. 8, no. 2, pp. 259-269, June 1947.

[11] S. I. H. Shah, S. M. Radha, P. Park, and I. J. Yoon, "Recent Advancements in Quasi-Isotropic Antennas: A Review," IEEE Access, vol. 9, pp. 146296-146317, 2021, doi: 10.1109/ACCESS.2021.3122181.

[12] M. F. Farooqui, C. Claudel, and A. Shamim, " An Electrically Small Spherical UHF d Buoyant 3-D Lagrangian Sensor for Real-Time Flood Monitoring," IEEE Transactions on Antennas and Propagation, vol. 62, no. 6, pp. 3354-3359, 2014, doi: 10.1109/TAP.2014.2309957.

[13] Z. Su, K. Klionovski, R. M. Bilal, and A. Shamim, "A Dual Band Additively Manufactured 3-D Antenna on Package With Near-Isotropic Radiation Pattern," IEEE Transactions on Antennas and Propagation, vol. 66, no. 7, pp. 3295-3305, 2018, doi: 10.1109/TAP.2018.2823729.

[14] P. Liu and Y. Li, "Quasi-Isotropic Radiation Pattern Synthesis Using Triple Current Line Sources," IEEE Transactions on Antennas and Propagation, vol. 68, no. 12, pp. 8150-8155, 2020, doi: 10.1109/TAP.2020.2995299.

[15] H. Ryu, G. Jung, D. Ju, S. Lim, and J. Woo, " A Low-Profile Antenna With Quasi RFID Tag Antenna With Quasi-Isotropic Patterns for Wireless Sensor Networks," Ieee Antenn Wirel Pr, vol. 9, pp. 60-62, 2010, doi: 10.1109/LAWP.2010.2043046.

[16] G. Pan, Y. Li, Z. Zhang, and Z. Feng, "Isotropic Radiation From a Compact Planar Antenna Using Two Crossed Dipoles," Ieee Antenn Wirel Pr, vol. 11, pp. 1338-1341, 2012, doi: 10.1109/LAWP.2012.2227450.

[17] J. Kim and S. Nam, "A Compact Quasi-Isotropic Antenna Based on Folded Split-Ring Resonators," Ieee Antenn Wirel Pr, vol. 16, pp. 294-297, 2017, doi: 10.1109/LAWP.2016.2573849.

[18] H. Liao, Q. Zhang, M. A. Karimi, Y. Kuo, N. Mishra, and A. Shamim, "An Additively Manufactured 3-D Antenna-in-Package With Quasi-Isotropic Radiation for Marine Animals Monitoring System," Ieee Antenn Wirel Pr, vol. 18, no. 11, pp. 2384-2388, 2019, doi: 10.1109/LAWP.2019.2937507.

[19] J. Ouyang, Y. M. Pan, S. Y. Zheng, and P. F. Hu, "An Electrically Small Planar Quasi-Isotropic Antenna," Ieee Antenn Wirel Pr, vol. 17, no. 2, pp. 303-306, 2018, doi: 10.1109/LAWP.2017.2787720.

[20] Y. Wang et al., "Design of Low-Cost, Flexible, Uniplanar, Electrically Small, Quasi-Isotropic Antenna," Ieee Antenn Wirel Pr, vol. 18, no. 8, pp. 1646-1650, 2019, doi: 10.1109/LAWP.2019.2925936.

[21] S. Long, "A combination of linear and slot antennas for quasi-isotropic coverage," IEEE Transactions on Antennas and Propagation, vol. 23, no. 4, pp. 572-576, 1975, doi: 10.1109/TAP.1975.1141121.

[22] L. Liang and S. V. Hum, "A Low-Profile Antenna With Quasi-Isotropic Pattern for UHF RFID Applications," Ieee Antenn Wirel Pr, vol. 12, pp. 210-213, 2013, doi: 10.1109/LAWP.2013.2245393.

[23] B. Wang, S. W. Cheung, W. Wang, M. Li, and T. I. Yuk, "A broadband and wide beamwidth dual circularly polarized antenna using crossed bent dipoles," in 2017 11th European Conference on Antennas and Propagation (EUCAP), 19-24 March 2017 2017, pp. 1936-1939, doi: 10.23919/EuCAP.2017.7928048. [Online]. Available: https://ieeexplore.ieee.org/document/7928048/

[24] X. He, L. Chang, and L. Chen, "A multifunction broad-beam antenna with dual bands and dual circular-polarizations," in 2016 IEEE MTT-S International Wireless Symposium (IWS), 14-16 March 2016 2016, pp. 1-4, doi: 10.1109/IEEE-IWS.2016.7585426. [Online]. Available: https://ieeexplore.ieee.org/document/7585426/

[25] K. Saurav, D. Sarkar, A. Singh, and K. V. Srivastava, "Multiband Circularly Polarized Cavity-Backed Crossed Dipole Antenna," IEEE Transactions on Antennas and Propagation, vol. 63, no. 10, pp. 4286-4296, 2015, doi: 10.1109/TAP.2015.2459131.

[26] G. Aijun, Y. Shiwen, and N. Zaiping, "Analysis and design of miniaturized ultra-wideband conical log spiral antennas," in 2013 Cross Strait Quad-Regional Radio Science and Wireless Technology Conference, 21-25 July 2013 2013, pp. 191-194, doi: 10.1109/CSQRWC.2013.6657385. [Online]. Available: https://ieeexplore.ieee.org/document/6657385/

[27] V. Galindo and K. Green, "A near-isotropic circulary polarized antenna for space vehicles," IEEE Transactions on Antennas and Propagation, vol. 13, no. 6, pp. 872-877, 1965, doi: 10.1109/TAP.1965.1138572.

[28] M. Huchard, C. Delaveaud, and S. Tedjini, "Miniature Antenna for Circularly Polarized Quasi Isotropic Coverage," in The Second European Conference on Antennas and Propagation, EuCAP 2007, 11-16 Nov. 2007 2007, pp. 1-5, doi: 10.1049/ic.2007.0953. [Online]. Available: https://ieeexplore.ieee.org/document/4458268

[29] H. H. Tran, S. X. Ta, and I. Park, "A Compact Circularly Polarized Crossed-Dipole Antenna for an RFID Tag," Ieee Antenn Wirel Pr, vol. 14, pp. 674-677, 2015, doi: 10.1109/LAWP.2014.2376945.

[30] S. Choi and K. Sarabandi, "A W-Shaped Antenna With Spatial Polarization Variation for Direction Finding," Ieee Antenn Wirel Pr, vol. 17, no. 12, pp. 2429-2433, 2018, doi: 10.1109/LAWP.2018.2877451.

[31] Z. Su, K. Klionovski, H. Liao, Y. Chen, A. Elsherbeni, and A. Shamim, "Antenna-on-Package Design: Achieving Near-Isotropic Radiation Pattern and Wide CP Coverage Simultaneously," IEEE Transactions on Antennas and Propagation, 2020.

[32] Z. Su, K. Klionovski, H. Liao, A. Shamim, Y. Chen, and A. Elsherbeni, "3D Antenna in Package Design: Maximizing Radiation Pattern Isotropicity and CP Coverage," in 2020 IEEE International Symposium on Antennas and Propagation and North American Radio Science Meeting, 5-10 July 2020 2020, pp. 263-264, doi: 10.1109/IEEECONF35879.2020.9330011. [Online]. Available: https://ieeexplore.ieee.org/document/9330011/

[33] D. Bugnolo, "A quasi-"Isotropic" antenna in the microwave spectrum," IRE Transactions on Antennas and Propagation,

vol. 10, no. 4, pp. 377-383, 1962, doi: 10.1109/TAP.1962.1137897.

[34] C. Wu and T. Ma, "Miniaturized Self-Oscillating Active Integrated Antenna with Quasi-Isotropic Radiation," IEEE Transactions on Antennas and Propagation, vol. 62, no. 2, pp. 933-936, 2014, doi: 10.1109/TAP.2013.2289942.

[35] J. W. Luo, Y. M. Pan, S. Y. Zheng, and S. H. Wang, "A Planar Angled-Dipole Antenna With Quasi-Isotropic Radiation Pattern," IEEE Transactions on Antennas and Propagation, vol. 68, no. 7, pp. 5646-5651, 2020, doi: 10.1109/TAP.2020.2963898.

[36] J. Kim, J. Park, A. A. Omar, and W. Hong, "A Symmetrically Stacked Planar Antenna Concept Exhibiting Quasi-Isotropic Radiation Coverage," Ieee Antenn Wirel Pr, vol. 19, no. 8, pp. 1390-1394, 2020, doi: 10.1109/LAWP.2020.3003011.

[37] C. Deng, Y. Li, Z. Zhang, and Z. Feng, "A Wideband Isotropic Radiated Planar Antenna Using Sequential Rotated L-Shaped Monopoles," IEEE Transactions on Antennas and Propagation, vol. 62, no. 3, pp. 1461-1464, 2014, doi: 10.1109/TAP.2013.2293787.

[38] C. A. Balanis, Antenna theory: analysis and design. John wiley & sons, 2016.

[39] H. F. Abutarboush and A. Shamim, "A Reconfigurable Inkjet-Printed Antenna on Paper Substrate for Wireless Applications," Ieee Antenn Wirel Pr, vol. 17, no. 9, pp. 1648-1651, 2018, doi: 10.1109/LAWP.2018.2861386.